ISSN No:-2456-2165 https://doi.org/10.38124/ijisrt/26aug585

Integrated Numerical Analysis of the Structural Behavior of a Multi-Span Prestressed Concrete Bridge under Road Traffic Loads and Time-Dependent Effects: A Case Study of the Bantoum Bridge, Cameroon

Nie Noumsi Thierry Constant[1]; Kayimbo Kamga Cyrille[1]; Guimezap Kenou Willy Chance[2]; Tatchum Defo Ulrich Giresse[3]; Bakam Stela[1]; Madja Doumbaye Jeremie[4]

[1]Fotso Victor University Institute of Technology, Civil Engineering Department, Research Unit of Industrial Systems and Engineering Environment (UR-ISIE), University of Dschang, Dschang, Cameroon
[2]School of Engineering and Applied Sciences, Institut Universitaire de la Cote, Douala, Cameroon
[3]Mechanics and Adapted Materials Laboratory (LAMMA), University of Douala, Douala, Cameroon
[4]National Advanced School of Engineering, Civil Engineering Department, University of Yaounde, Yaounde, Cameroon

Publication Date: 2026/08/29

Abstract: Assessing the performance of multi-span prestressed concrete bridges requires the combined consideration of traffic-induced actions, prestressing, the mechanical properties of materials, and the time-dependent effects of concrete. This study investigates the structural behavior of the deck of the Bantoum River Bridge, located along National Road RN4 in Cameroon. The bridge consists of five 30-m spans, four prestressed concrete main girders, and a reinforced concrete deck slab. A three-dimensional numerical model was developed using MIDAS Civil 2022 based on the actual geometry of the structure, the mechanical properties of the materials, the support conditions, and the prescribed design actions. The LM1 and LM3 road traffic load models, wind actions, and time-dependent effects associated with concrete creep and shrinkage were considered. The results show that the most highly loaded main girder reaches a maximum bending moment of 8.9423 MN.m and a maximum shear force of 1.3176 MN at the ultimate limit state (ULS). The design leads to the adoption of four 12T15 prestressing tendons and a minimum required prestressing force of 7.07 MN. The verification results show that the maximum stresses in the concrete, prestressing steel, and passive reinforcement remain below the adopted limits. The analysis of time-dependent effects further indicates a final creep coefficient of 1.8549 and a shrinkage strain of -2.7539×10^{-4}. These results show that the combined consideration of traffic actions, prestressing, and time-dependent phenomena provides a more comprehensive characterization of the structural behavior of the bridge deck under the considered design conditions.

Keywords: *Multi-Span Bridge; Prestressed Concrete; Numerical Analysis; Road Traffic Loads; Structural Behavior.*

How to Cite: Nie Noumsi Thierry Constant; Kayimbo Kamga Cyrille; Guimezap Kenou Willy Chance; Tatchum Defo Ulrich Giresse; Bakam Stela; Madja Doumbaye Jeremie (2026) Integrated Numerical Analysis of the Structural Behavior of a Multi-Span Prestressed Concrete Bridge under Road Traffic Loads and Time-Dependent Effects: A Case Study of the Bantoum Bridge, Cameroon. *International Journal of Innovative Science and Research Technology*, 11(8), 1899-1912. https://doi.org/10.38124/ijisrt/26aug585

I. INTRODUCTION

Bridges and other crossing infrastructures are key components of transportation networks, as they ensure the continuity of traffic across natural obstacles such as rivers, valleys, and rugged terrain. Within this category, bridges play a central role in connecting territories, facilitating traffic flow, and supporting socioeconomic development. Their design must simultaneously satisfy requirements related to safety, durability, serviceability, and material efficiency, while accounting for operating conditions and the local environment. The selection of a structural system depends on

ISSN No:-2456-2165 https://doi.org/10.38124/ijisrt/26aug585

numerous parameters, including span length, traffic conditions, site characteristics, and maintenance constraints. For medium- to long-span structures, prestressed concrete is particularly suitable because of its ability to introduce a predetermined compressive stress into the concrete. This compression helps limit tensile stresses and cracking, control service-level deformations, and optimize the dimensions of load-bearing sections. Prestressing therefore contributes to improving the structural efficiency of load-bearing members while satisfying strength and serviceability requirements.

The development of modern prestressing is closely associated with the work of Eugène Freyssinet, whose research notably highlighted the importance of shrinkage and creep in the long-term behavior of concrete and in maintaining the effectiveness of prestressing (Hewson, 2011; Freyssinet, 1966). These time-dependent phenomena are essential mechanisms governing the evolution of deformation and stress states in prestressed structures. Their consideration is therefore necessary for an appropriate assessment of structural behavior beyond the instantaneous response. Since its development, prestressed concrete has become widely used in civil engineering structures, particularly bridges, for which ultimate and serviceability limit-state verifications are essential stages of structural design. Within the European regulatory framework, Eurocode 0 establishes the general basis of structural design, Eurocode 1 specifies the actions to be considered, and Eurocode 2 provides the design rules for concrete structures (CEN, 2003; CEN, 2005; CEN, 2006). For bridge structures, these provisions are complemented by specific requirements concerning road traffic loads, load combinations, and long-term structural behavior. Beyond strength verification, the analysis of a prestressed concrete bridge must account for the interaction between operational actions, structural stiffness, the prestressing level, and the time-dependent behavior of concrete. Road traffic loads may generate varying structural demands depending on their longitudinal and transverse positions on the deck, whereas creep and shrinkage progressively modify the deformation state of the concrete and contribute to changes in the effective prestressing force. Numerical assessment of these mechanisms therefore provides a relevant approach for characterizing the structural behavior of a multi-span bridge deck.

In the Cameroonian context, increasing traffic on major road corridors reinforces the need for rigorous assessment of existing structures and infrastructure intended to ensure the long-term continuity of transportation networks. The Bantoum River Bridge, located along RN4 in the Western Region of Cameroon, is a structure of particular technical and operational interest. Its investigation provides an opportunity to examine the behavior of a multi-span prestressed concrete bridge deck under the geometric and regulatory conditions associated with an actual structure. Despite the importance of this type of infrastructure, detailed studies addressing the mechanical response of the Bantoum Bridge and the integrated assessment of its structural performance remain limited. Available studies on prestressed bridges mainly address long-term behavior, creep and shrinkage effects, reliability, or the influence of traffic loads, whereas these approaches are rarely applied jointly to an actual structure within the Cameroonian road network. This research gap justifies an approach combining numerical modeling of the structure, assessment of structural demands induced by road traffic and environmental actions, design of prestressing and passive reinforcement, and consideration of the time-dependent effects of concrete. In this context, it is relevant to develop an integrated numerical model accounting for road traffic actions, prestressing, and time-dependent effects of concrete in order to characterize the structural demands, design requirements, and serviceability performance of the multi-span deck of the Bantoum Bridge.

The objective of this study is to assess the structural behavior of the deck of the multi-span Bantoum Bridge through three-dimensional numerical modeling and structural design in accordance with the adopted regulatory provisions. More specifically, the study aims to determine the internal forces under the various loading configurations, evaluate the effects of concrete creep and shrinkage, design the prestressing system and passive reinforcement of the structural members, and subsequently verify the stresses and deformations at the ultimate and serviceability limit states. The analysis therefore seeks to identify the mechanisms governing the structural response of the deck and to assess its compliance with the adopted design criteria under the considered operating conditions.

II. LITERATURE REVIEW

➢ *Development and Principles of Prestressed Concrete*

Prestressed concrete has become a major structural solution for medium- and long-span bridges because of its ability to introduce a predetermined compressive stress into concrete, thereby limiting tensile stresses induced by service loads. This technique helps reduce cracking, control service-level deformations, and improve the structural efficiency of load-bearing sections. The development of modern prestressing is closely associated with the work of Eugène Freyssinet. His research contributed notably to highlighting the decisive role of concrete creep and shrinkage in maintaining prestressing tension and governing the long-term behavior of prestressed structures (Freyssinet, 1950; Hewson, 2011). The early difficulties encountered in the application of prestressing demonstrated that the effectiveness of a prestressing system could not be assessed solely from its initial stressing condition, but had to account for the evolution of concrete properties and prestress losses over time.

This historical development led to the establishment of design methods capable of considering ultimate and serviceability limit states simultaneously. For prestressed concrete bridges, design must therefore be based not only on the load-bearing capacity of structural sections but also on the control of stresses, deformations, and cracking throughout the different stages of the bridge's service life.

➢ *Regulatory Framework for the Design of Prestressed Bridges*

The design of prestressed concrete structures is currently governed by the Eurocodes. EN 1990 establishes

ISSN No:-2456-2165 https://doi.org/10.38124/ijisrt/26aug585

the basis of structural design and the general principles governing limit states and load combinations (CEN, 2003). EN 1992-1-1 provides general design rules for concrete structures, while EN 1992-2 specifies provisions applicable to concrete bridges, particularly with regard to strength, serviceability, and detailing requirements (CEN, 2005; CEN, 2006). The provisions applicable to bridges must be combined with an appropriate definition of traffic loads, permanent actions, and environmental actions. The analysis must also account for the different stages of structural behavior, from tendon stressing to the long-term state. Shrinkage and creep effects must in particular be incorporated into serviceability verifications because they progressively modify concrete deformations and the effective prestressing state (CEN, 2007).

Within this framework, the design of a prestressed bridge cannot therefore be reduced to an isolated flexural strength verification. It must be regarded as an integrated process combining the geometric characteristics of the deck, material properties, applied actions, initial and effective prestressing, prestress losses, and the time-dependent effects of concrete.

- *Time-Dependent Effects and Long-Term Behavior*

Time-dependent phenomena constitute one of the major challenges governing the long-term behavior of prestressed concrete structures. Creep refers to the progressive increase in concrete strain under sustained stress, whereas shrinkage represents the contraction of concrete independently of the presence of mechanical loading. In prestressed structures, these two mechanisms can modify the stress state of concrete and contribute to long-term prestress losses. Several studies have shown that these phenomena can significantly influence the long-term deformations of prestressed bridges. Nguyen et al. (2022) investigated the influence of creep and shrinkage models on the prediction of long-term deflection in a three-span prestressed concrete bridge. Their results show that the choice of the time-dependent behavior model can significantly affect the assessment of final deformations. This observation is particularly relevant for multi-span structures, in which time-dependent effects may interact with the structural configuration.

Li et al. (2019) also investigated the three-dimensional nonlinear effects of creep and shrinkage in a long-span prestressed concrete box-girder bridge. Their findings highlight the importance of incorporating time-dependent effects into realistic modeling of prestressed structures, particularly when spatial variations in deformation may influence the global response of the structure.

In a complementary approach, Williams et al. (2024) experimentally investigated creep and shrinkage phenomena in prestressed concrete beams. Their results emphasize the importance of these mechanisms in the evolution of structural response and confirm the need to consider them when assessing long-term behavior. These findings are particularly relevant to the interpretation of numerical models applied to real structures.

Teng et al. (2016), in turn, analyzed the long-term performance of prestressed concrete bridges by simultaneously considering the effects of concrete damage, static creep, and traffic-induced cyclic creep. Their approach highlights the evolving nature of bridge response under repeated loading and emphasizes the value of an assessment framework that extends beyond instantaneous structural demands.

The literature therefore shows that time-dependent behavior is not a secondary effect in the analysis of prestressed bridges. It directly influences the evolution of deformations and effective prestressing and, consequently, the assessment of the bridge's serviceability performance.

- *Reliability, Serviceability, and Design of Prestressed Structures*

Beyond creep and shrinkage phenomena, in-service reliability represents another important aspect of prestressed bridge design. Cheng (2013) investigated the serviceability reliability of prestressed concrete bridges by considering uncertainties associated with structural parameters and applied loads. This approach shows that deterministic compliance with a design limit is not always sufficient to characterize the robustness of structural response.

Ghali and Elbadry (1989) also emphasized the importance of serviceability provisions in prestressed structures. Additional passive reinforcement does not contribute solely to overall strength; it also plays a role in crack control, local ductility, and detailing requirements. This consideration is particularly relevant to prestressed girders, in which prestressing constitutes the primary flexural resistance mechanism.

The work of Gilbert et al. (2017) further provides a reference framework for the design of prestressed structures in accordance with Eurocode 2 by relating regulatory design principles to the behavioral mechanisms of prestressed sections. These contributions reinforce the importance of an approach combining strength, serviceability, and structural detailing.

- *Numerical Modeling of Prestressed Bridges*

The development of numerical analysis tools has considerably improved the representation of the behavior of prestressed bridges. Numerical models can account for the three-dimensional geometry of the structure, different loading configurations, the distribution of structural demands among load-bearing members, and the evolution of structural response under time-dependent phenomena.

Luo et al. (2022) used numerical modeling to investigate the coupled behavior of a prestressed concrete bridge under the effects of time-dependent deformations. Their study illustrates the value of numerical models for analyzing the influence of long-term behavior on the global structural response. Similarly, Li et al. (2019) showed that accounting for the three-dimensional effects of creep and shrinkage can modify the response of a prestressed bridge and

ISSN No:-2456-2165 https://doi.org/10.38124/ijisrt/26aug585

therefore justifies the use of numerical models that adequately represent the geometry and actual structural behavior.

Numerical modeling is therefore particularly valuable for multi-span bridges because it enables the simultaneous investigation of longitudinal structural demands, transverse load distribution, the response of the main girders and deck slab, and the evolution of deformations over time.

The analysis of previous studies highlights three main findings. First, the behavior of prestressed concrete bridges strongly depends on the interaction between applied actions, prestressing, and the mechanical properties of concrete. Second, time-dependent phenomena, particularly creep and shrinkage, can significantly modify long-term deformations and prestress losses; their consideration is therefore essential for a realistic assessment of serviceability performance (Nguyen et al., 2022; Li et al., 2019; Williams et al., 2024). Third, numerical modeling provides an appropriate framework for simultaneously incorporating these different mechanisms and analyzing their influence on the global response of bridges. However, the studies reviewed in this manuscript mainly concern continuous bridges, multi-span bridges, or prestressed beams investigated under specific configurations and conditions. The available results therefore do not, by themselves, provide a basis for characterizing the behavior of an actual structure with the geometric characteristics and operating conditions of the Bantoum River Bridge. The positioning of the present study therefore lies in applying an integrated numerical approach to an actual multi-span prestressed concrete bridge located in Cameroon. The approach combines the actual deck geometry, permanent and variable actions, road traffic loads, prestressing, creep and shrinkage effects, and ultimate and serviceability limit-state verifications. The objective is therefore not merely to verify the structural strength of the bridge, but also to identify the mechanisms governing its response and assess the influence of time-dependent phenomena on its in-service behavior.

This approach extends existing research by providing an analysis applied to an actual structure within the Cameroonian context, while establishing a relationship between numerically determined structural demands, the design of prestressing and reinforcement, and the structural performance criteria specified by the adopted design standards.

III. MATERIALS AND METHODS

➢ *Description of the Structure and Study Site*

The study focuses on the bridge crossing the Bantoum River, located along National Road RN4 in the Ndé Department, Western Region of Cameroon. The structure is located within the municipality of Bangangté, in the village of Bantoum, and constitutes an important road infrastructure for maintaining connectivity between the main economic centers served by this road corridor.

The geographical location of the study site is presented in Figure 1.

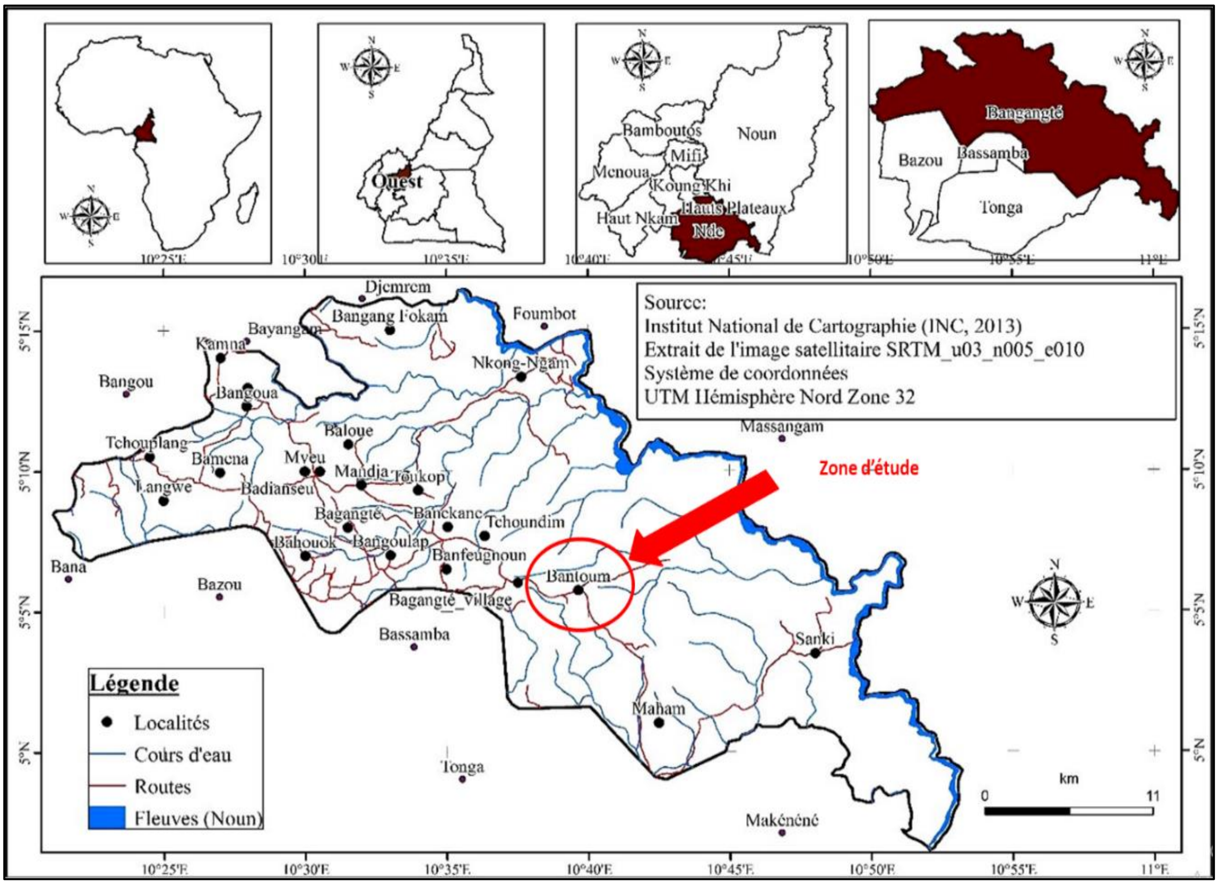

Fig 1 Location of the Study Area.

ISSN No:-2456-2165 https://doi.org/10.38124/ijisrt/26aug585

Figure 2 presents an aerial view of the bridge and its immediate surroundings. The bridge consists of five 30-m spans, corresponding to a total length of 150 m. The deck is supported by four prestressed concrete main girders carrying a reinforced concrete deck slab. The total deck width is 9.60 m, and the bridge accommodates two traffic lanes.

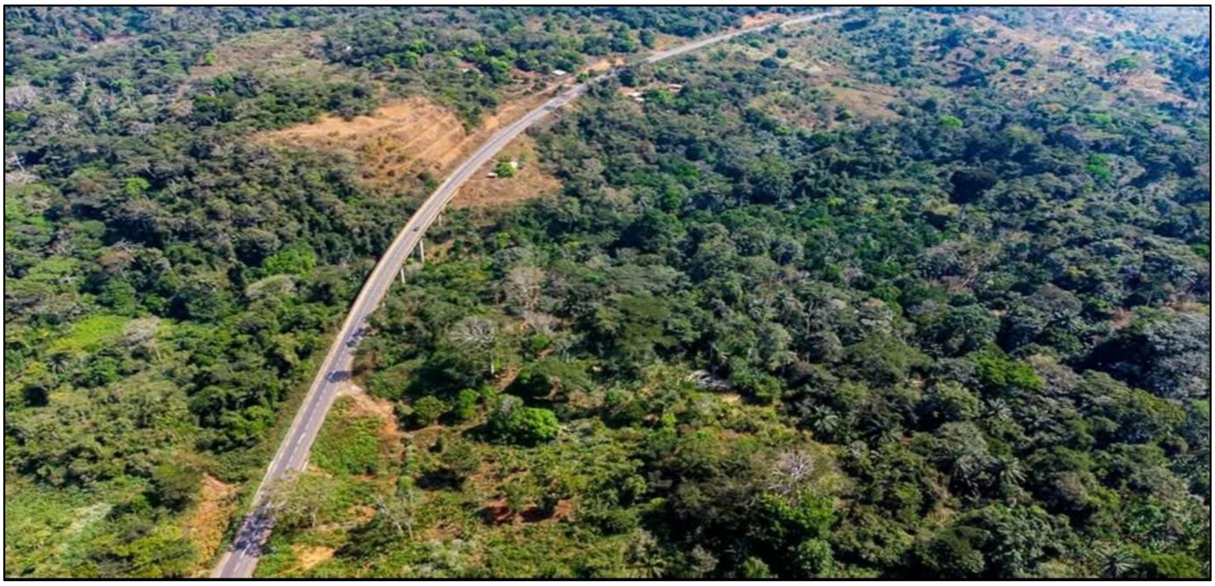

Fig 2 Aerial View of the Bridge Over the Bantoum River.

The study is deliberately focused on the structural behavior of the bridge deck. The piers, bearings, and foundations are not designed or dimensioned as part of the present study.

➢ *Data Collection and Characterization*

The data required for the analysis were collected from the technical project documents provided by the Ministry of Public Works, together with the available documentation on the structure. These data comprise two main categories: geometric data and structural data. The geometric data were obtained from the longitudinal and transverse drawings of the bridge and were used to define the spatial configuration and dimensions of the various deck components. The structural data include, in particular, the mechanical properties of the materials, support conditions, characteristics of the load-bearing members, and the parameters required for regulatory verifications.

➢ *Deck Geometry and Preliminary Design*

The preliminary design was carried out based on the geometric characteristics of the structure and focused on the main girders, cross-beams, and deck slab. The selected dimensions constitute the reference geometric data used for the numerical modeling.

The main characteristics of the bridge are summarized in Table 1.

Table 1 Main Geometric Characteristics of the Bridge.

Description	**Value**	**Unit**
Total bridge length	150	m
Number of spans	5	–
Span length	30	m
Total deck depth	1.80	m
Cap beam cross-section	150 × 150	cm²
Number of main girders	4	–
Bridge width	9.60	m
Sidewalk width	1.20	m

The detailed preliminary design of the different deck components is presented in Table 2.

Table 2 Reference Dimensions of the Deck Components.

Element	**Dimension**		**Value and unit**
Deck (girder + slab)	Total depth		$h_t = 180$ cm
Top flange	Width		$b_T = 110$ cm
	Thickness		$e_T = 15$ cm
	Gusset	In the mid-span region	$(\alpha_m = 45°, e_{\alpha m} = 10$ cm$)$ $(\beta_m = 8.1°, e_{\beta m} = 5$ cm$)$

ISSN No:-2456-2165 https://doi.org/10.38124/ijisrt/26aug585

		At supports	($\beta_m = 8.1°$, $e_{\beta m} = 3.57$cm)
Web	Thickness	In the mid-span region	$e_{web\_\_m} = 20$ cm
		At supports	$e_{web\_a} = 60$ cm
Haunch	Width		$b_t = 60$ cm
	Thickness		$e_t = 15$ cm
	Gusset	In the mid-span region	($\alpha_t = 45°$, $e_{\alpha t} = 20$ cm)
		At supports	/
Girder	Spacing		$\lambda = 235$ cm
Deck slab	Width		$l_h = 235$ cm
	Thickness		$h_h = 20$ cm
Girder	Height		$h_p = 160$ cm
Cross-beam	Height		$h_e = 140$ cm
	Thickness		$e_e = 30$ cm
Sidewalk	Width		$l_t = 120$ cm
	Thickness		$e_t = 25$ cm

The adopted geometry consists of four main girders spaced at 2.35 m and connected to a 20-cm-thick deck slab. The other section dimensions, including those of the top flange, web, bottom flange, cross-beams, and sidewalks, are those given in Table 2.

Figure 3 presents the transverse cross-section adopted for the numerical modeling.

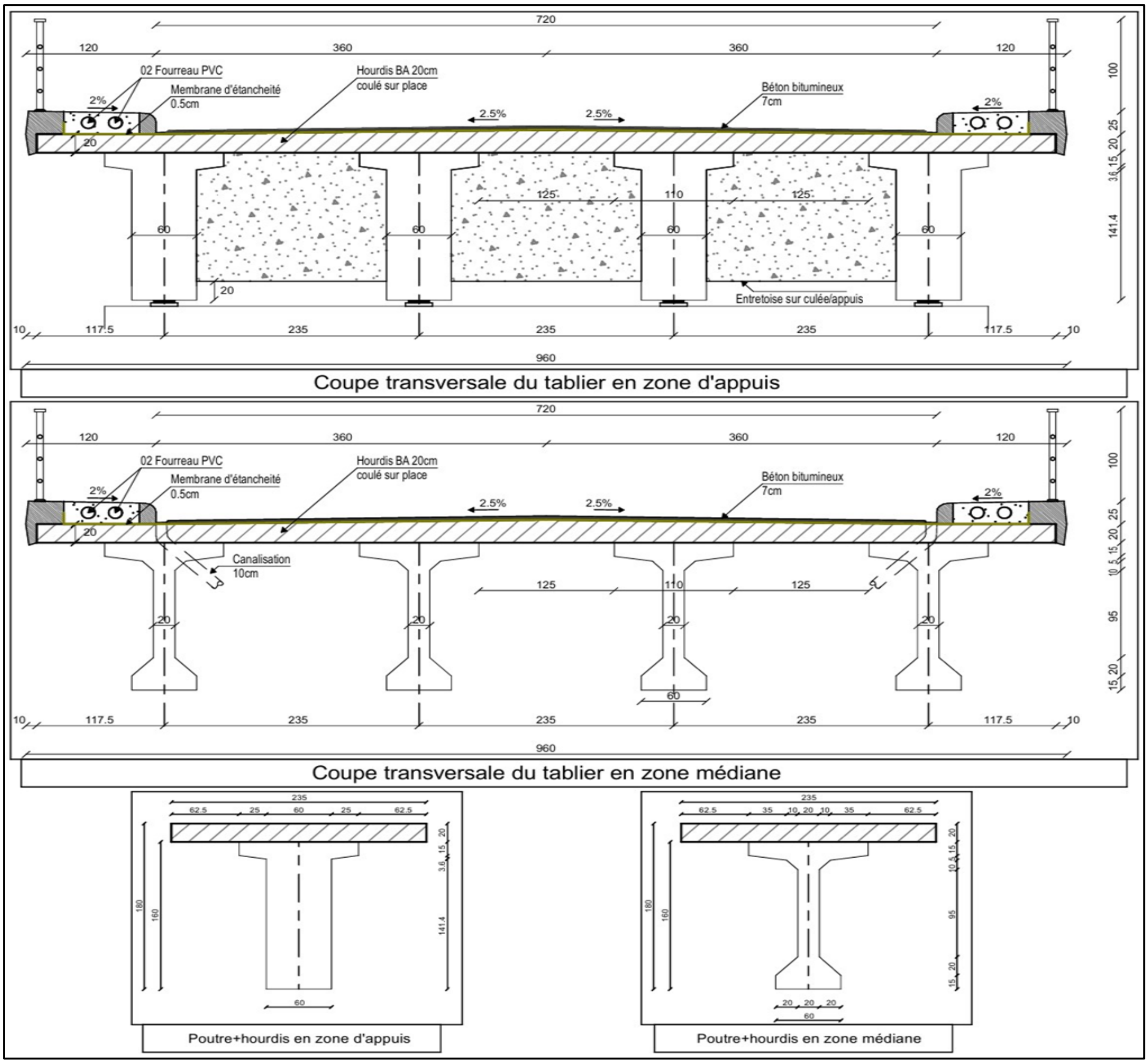

Fig 3 Transverse Cross-Section of the Bridge Deck.

ISSN No:-2456-2165 https://doi.org/10.38124/ijisrt/26aug585

➢ *Regulatory Framework*

The design is carried out in accordance with the provisions of the Eurocodes applicable to concrete structures and bridges. Eurocode 0 is used for the general principles of structural design and load combinations, Eurocode 1 for the definition of actions, and Eurocode 2 for the design of concrete structures. For bridge components, the specific provisions of Eurocode 2, Part 2, are adopted. Loads and testing requirements applicable to road bridges are also considered in accordance with Fascicule 61, Title II of the CPC. This regulatory framework is consistent with the literature on the design of prestressed bridges, in which ultimate and serviceability limit-state verifications constitute the main criteria for assessing structural performance (CEN, 2003, 2005, 2006; CEN, 2007).

➢ *Traffic Actions*

The operational loads acting on the deck are defined based on the LM1 and LM3 load systems. The LM1 system represents standard road traffic loading conditions and includes concentrated loads from the tandem system together with uniformly distributed loads. The values used for the different traffic lanes and residual areas are given in Table 3.

Table 3 Loads of the LM1 system.

Location	**TS: q_k (kN)**	**α_{q_i}**	**TS (kN)**	**UDL: q_k (kN/m²)**	**α_{q_i}, α_{q_r}**	**Lane width (m)**	**UDL: q_k (kN/m)**
Lane No. 1	300	1	300	9	1	3	27
Lane No. 2	200	1	200	2.5	1	3	7.5
Residual area 1	0	1	0	2.5	1	0.6	1.5
Residual area 2	0	1	0	2.5	1	0.6	1.5

For Lane No. 1, the adopted concentrated load is 300 kN and the corresponding uniformly distributed load is 27 kN/m. For Lane No. 2, the corresponding values are 200 kN and 7.5 kN/m, respectively. The residual areas are subjected to the corresponding loads defined in Table 3. The LM3 system is introduced to account for heavy-traffic loading conditions. The configurations considered include the Mc120, Me120, and timber truck (*grumier*) vehicles.

Table 4 Loads of the LM3 system.

LM3 load system			
Subsystem	**Total overload (kN)**	**δ**	**Value used (kN)**
Mc120	1100	1.44	1584
Me120	660	1.44	950.4
Timber truck	1000	1.44	1440

After application of the factor ($\delta = 1.44$), the values used are 1584 kN for Mc120, 950.4 kN for Me120, and 1440 kN for the timber truck, respectively. The simultaneous consideration of LM1 and LM3 therefore makes it possible to assess the deck response under loading configurations representative of the different traffic situations considered in the study.

➢ *Wind Action*

The wind action is determined from the exposed geometry of the deck and the adopted aerodynamic parameters. The calculation parameters and resulting force are summarized in Table 5.

Table 5 Parameters and Results of the Wind Action Calculation.

Parameter	**Symbol**	**Value**	**Unit**
Total depth	d_{tot}	3.05	m
Width-to-depth ratio	b/d_{tot}	3.21	–
Reference area	A_{ref}	79.5	m²
Exposure factor	c_e	0.0018	–
Wind force coefficient	c_f	1.54	–
Wind load factor	C	0.0027	–
Wind force on the element	F_w	64.93	kN
Distributed wind load	P	2.16	kN/m

The total depth considered is 3.05 m and the reference area is 79.5 m². The adopted force coefficient is ($c_f = 1.54$). The calculation gives a global wind force of 64.93 kN, corresponding to a distributed load of 2.16 kN/m. This action is subsequently incorporated into the design load combinations in accordance with the adopted regulatory framework.

➢ *Numerical Modeling*

The bridge deck is modeled using MIDAS Civil 2022 based on the actual geometry of the structure, the mechanical properties of the materials, the support conditions, the load cases, and the regulatory load combinations. The analysis is performed under linear static conditions to evaluate the deck response under the different actions considered.

ISSN No:-2456-2165 https://doi.org/10.38124/ijisrt/26aug585

The model accounts for permanent actions, LM1 and LM3 road traffic loads, wind action, and time-dependent effects associated with concrete shrinkage and creep. The model geometry is defined from the dimensions presented in Tables 1 and 2 and the transverse cross-section shown in Figure 3. This approach ensures consistency between the geometric data of the structure and the assumptions adopted for the numerical analysis.

➢ *Consideration of Time-Dependent Effects*

The time-dependent effects of concrete are considered through creep and shrinkage. The calculation parameters are defined for a relative humidity of 80%, with creep beginning three days after casting. The purpose of incorporating these effects is to assess the long-term evolution of the deck response and, in particular, their influence on structural deformations and the stress state of the prestressed structure.

➢ *Verification Procedure*

The structural demands obtained from the numerical model are used for the design of the prestressing system, the passive reinforcement of the main girders, and the reinforcement of the deck slab. The verifications cover: flexural resistance; shear resistance; stresses in concrete; stresses in prestressing steel; stresses in passive reinforcement; design moments in the slab; structural deformations and deck deflection. The verifications are performed at the ultimate and serviceability limit states, in accordance with the regulatory framework defined above.

IV. RESULTS AND DISCUSSION

➢ *Global Response of the Main Girders*

The numerical analysis provides the envelopes of the structural demands in the main girders under the different design load combinations. The results are summarized in Tables 6 and 7.

Table 6 Envelopes of Structural Demands in the Main Girders.

	ULS –ENV		SLS_k–ENV	SLS_f–ENV	SLS_{qp}–ENV
	M_{Ed} (MN. m)	V_{Ed} (MN)	M_{Ed} (MN. m)	M_{Ed} (MN. m)	M_{Ed} (MN. m)
Maximum value (+)	8.9423	1.3176	6.4338	5.7349	4.2481
Minimum value (−)	0.2848	1.2796	0.1960	0.1563	0.1171

Table 7 Summary of ULS and SLS Structural Demands in the Main Girders.

ULS–ENV		**SLS_k–ENV**	**SLS_f–ENV**	**SLS_{qp}–ENV**
M_{Ed} (MN. m)	**V_{Ed}(MN)**	**M_{Ed} (MN. m)**	**M_{Ed} (MN. m)**	**M_{Ed} (MN. m)**
8.9423	1.3176	6.4338	5.7349	4.2481

At the ultimate limit state, the maximum bending moment obtained is 8.9423 MN·m, associated with a maximum shear force of 1.3176 MN. At the serviceability limit state, the maximum bending moments reach 6.4338 MN·m for the characteristic combination, 5.7349 MN·m for the frequent combination, and 4.2481 MN·m for the quasi-permanent combination.

The distribution of structural demands indicates that the critical sections correspond to regions where the combined effects of permanent loads, traffic actions, and prestressing generate the highest structural demands.

Figure 4 simultaneously presents the bending-moment and shear-force diagrams of the most highly loaded main girder.

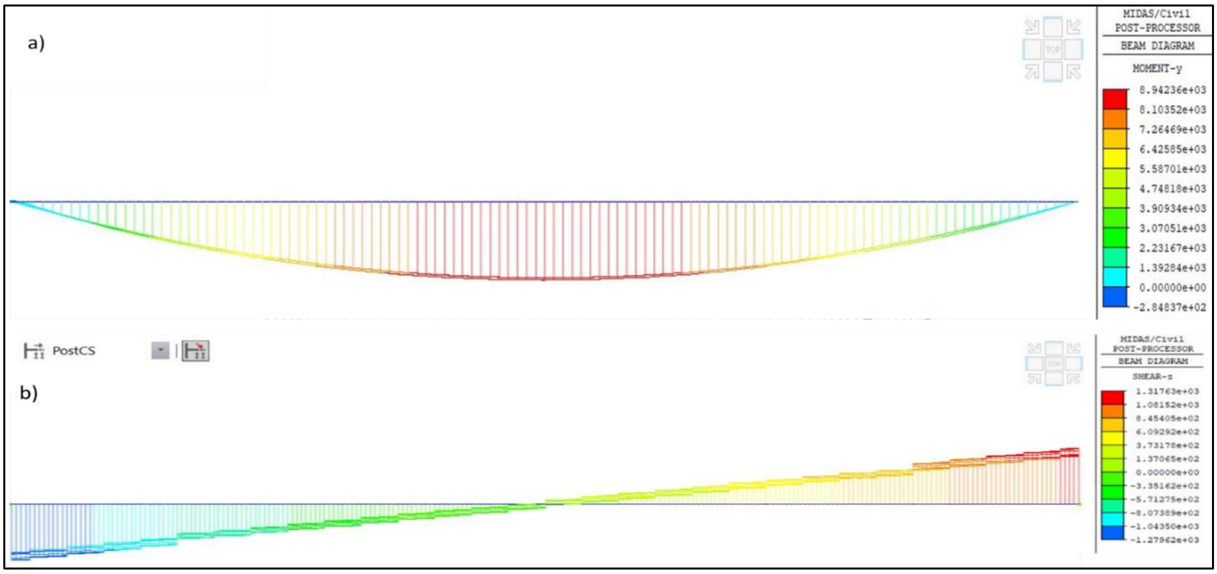

Fig 4 Bending Moment (a) and Shear Force (b) Diagrams of the Most Highly Loaded Main Girder Under the Envelope ULS Combination.

➢ *Prestressing Design*

The prestressing system is designed based on the maximum structural demands obtained above. The adopted system consists of 12T15 tendons made of prestressing steel with a characteristic tensile strength of (f_{pk}=1860) MPa. The conventional yield strength is ($f_{p0.1k}$=1581) MPa, and the nominal steel cross-sectional area per tendon is (A_p=1668) mm².

The determination of the maximum allowable stress is presented in Table 8.

Table 8 Prestressing Design Parameters.

Material	Parameter		Value
Concrete	Characteristic compressive strength		f_{ck} = 35 MPa
	Mean tensile strength of concrete		f_{ctm} = 3.2 MPa
	Allowable compressive stress	during construction ($\overline{\sigma_{c1}} = 0.6 \times f_{ck}$)	$\overline{\sigma_{c1}}$ = 21 MPa
		in service ($\overline{\sigma_{c2}} = 0.5 \times f_{ck}$)	$\overline{\sigma_{c2}}$= 17.5 MPa
	Allowable tensile stress	during construction ($\overline{\sigma_{t1}} = 0.7 \times f_{ctm}$)	$\overline{\sigma_{t1}}$ = -2.24 MPa
		in service	$\overline{\sigma_{t2}} = 0$
Prestressing steel	Adopted tendon type		12T15
	Characteristic tensile strength		f_{pk} = 1860 MPa
	Conventional yield strength		$f_{p0,1k}$ = 1581 MPa
	Nominal steel cross-sectional area		A_p= 1668 mm²
	Duct diameter		ϕ = 90 mm
	Maximum stress, $\sigma_{p,max}$ = min {0,8 × f_{pk}; 0,9 × $f_{p0,1k}$}		$\sigma_{p,max}$ = 1422.9 MPa
	Maximum prestressing force, $P_{max} = A_p \times \sigma_{p,max}$		P_{max}= 2.40 MN

The design results in the adoption of four 12T15 tendons, corresponding to the minimum required prestressing force of 7.07 MN for flexural resistance.

The selected prestressing arrangement is consistent with the level of structural demand obtained at the ULS. Prestressing constitutes the primary flexural resistance mechanism in this case, which also explains the limited requirement for additional tensile passive reinforcement.

➢ *Passive Reinforcement of the Main Girders*

Table 9 presents the design of the passive reinforcement of the main girders.

Table 9 Summary of the Passive Reinforcement Design of the Main Girders.

	Longitudinal reinforcement		
	Calculated area (mm²)	**Adopted area (mm²)**	**Bars**
Bottom longitudinal reinforcement	No additional passive tensile reinforcement is required for ultimate flexural resistance. However, the minimum passive reinforcement required in the tensile zone is provided, since the prestressing tendons alone ensure the ultimate flexural resistance.		
Tensile passive reinforcement (bottom region)	526	615.75	4HA14
Top longitudinal reinforcement	No compression reinforcement is required. Minimum reinforcement is provided for construction and detailing purposes.		
Upper reinforcement	307.87	452.38	4HA12
Skin reinforcement	1320	1809.55	8HA12/per face
	Transverse reinforcement		
Bar diameter Øt		Number of legs	Spacing St (mm)
HA12		4	350

No additional tensile passive reinforcement is required to ensure ultimate flexural resistance, as the prestressing tendons provide the main contribution to moment resistance. Nevertheless, a minimum reinforcement area of 526 mm² is retained in the tensile zone and increased to 615.75 mm², corresponding to 4HA14.

In the upper region, the calculated reinforcement area of 307.87 mm² is replaced by 452.38 mm², corresponding to 4HA12. The skin reinforcement, calculated as 1320 mm², is increased to 1809.55 mm², corresponding to 8HA12 per face. The transverse reinforcement consists of four-leg HA12 stirrups spaced at 350 mm.

The adoption of reinforcement areas greater than the calculated minimum requirements allows both structural requirements and the adopted detailing provisions to be satisfied.

➢ *Stress Verification in the Main Girders*

The stress verification results are presented in Table 10. The maximum stress in concrete is 17.91 MPa, compared

ISSN No:-2456-2165 https://doi.org/10.38124/ijisrt/26aug585

with an allowable limit of 21 MPa. The stress in the prestressing steel reaches 1151 MPa, compared with an allowable limit of 1422.9 MPa. The stress in the passive reinforcement is 90.66 MPa, compared with an allowable limit of 400 MPa.

The corresponding stress-to-allowable-limit ratios are approximately 0.85 for concrete, 0.81 for prestressing steel, and 0.23 for passive reinforcement, respectively.

These results indicate that the stress levels remain below the adopted limits for all three material categories. Concrete nevertheless exhibits the highest level of stress utilization among the three materials.

Table 10 Stress Verification in Concrete and Reinforcement of the Main Girders.

Material	Calculated stress σ (MPa)	Allowable limit $\bar{\sigma}$ (MPa)	Condition	Assessment
Concrete	17.91	21	$\sigma_c \leq \bar{\sigma}_c$	**Verified**
Prestressing steel	1151	1422.9	$\boldsymbol{\sigma_{pm}} \leq \overline{\sigma_{pm}}$	**Verified**
Passive reinforcement	90.66	400	$\sigma_s \leq \bar{\sigma}_s$	**Verified**

➢ *Time-Dependent Effects of Concrete*

The evolution of time-dependent behavior is presented in Figures 5 and 6 and summarized in Table 11.

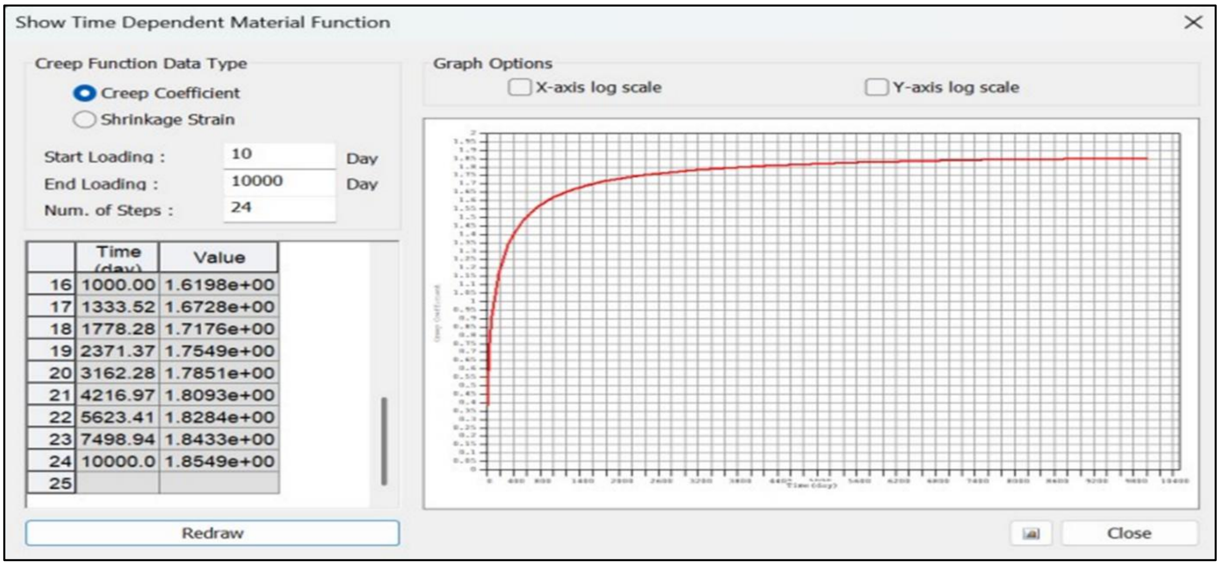

Fig 5 Evolution of the Concrete Creep Coefficient as a Function of Time.

The creep coefficient progressively increases with time and reaches an asymptotic value of 1.8549. This evolution highlights the significance of the viscoelastic behavior of concrete in the long-term assessment of the deck.

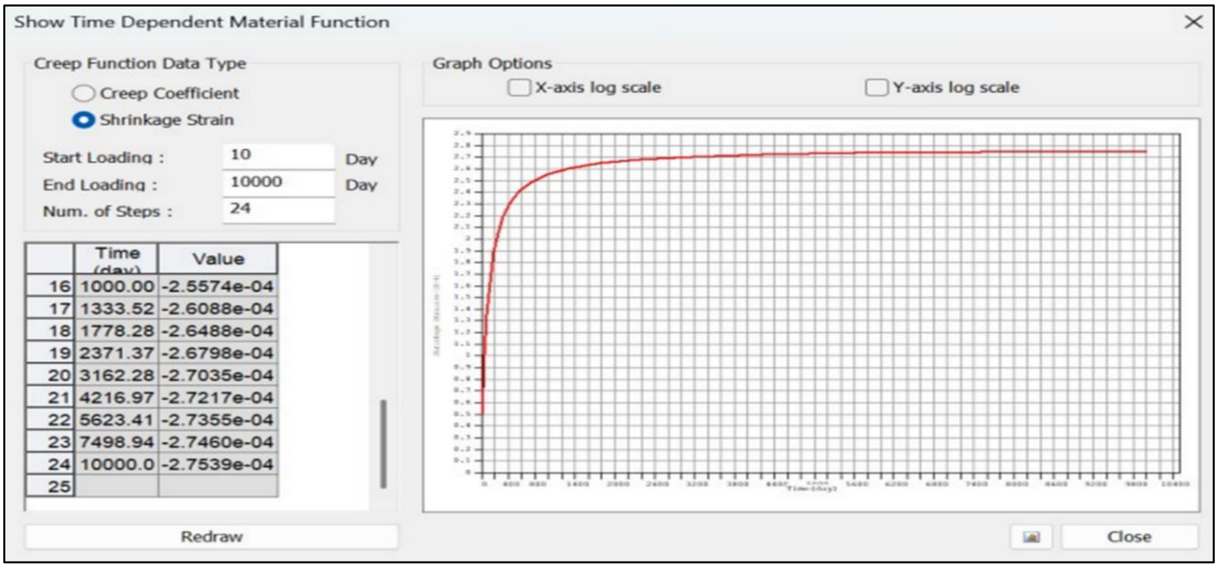

Fig 6 Evolution of Concrete Shrinkage Strain as a Function of Time.

ISSN No:-2456-2165 https://doi.org/10.38124/ijisrt/26aug585

The effective elastic modulus used for the time-dependent assessment is 11,909.34 N/mm², while the long-term creep coefficient is 1.8549 and the final shrinkage strain is -2.7539×10^{-4}, as reported in Table 11. These results indicate that time-dependent behavior cannot be neglected in the analysis of a prestressed bridge deck. Creep and shrinkage progressively modify the strain state of the concrete and may contribute to a reduction in the effective prestressing force available over time. This observation is consistent with the findings of Nguyen et al. (2022), Li et al. (2019), and Williams et al. (2024), who reported that creep and shrinkage models can significantly influence the prediction of long-term deformations in prestressed concrete structures.

Table 11 Parameters Obtained from the Creep and Shrinkage Analysis.

Description	Symbol	Value	Unit
Effective elastic modulus of concrete	E_c,eff	11,909.34	N/mm²
Long-term concrete creep coefficient	P (∞, t_0)	1.8549	–
Long-term concrete shrinkage strain	ε_{cs} (∞)	-2.7539×10^{-4}	–

➢ *Deck Slab Behavior*

The bending moments in the deck slab are presented in Tables 12 and 13.

Table 12 Maximum Bending Moments in the Deck Slab.

Bending moments M_{Ed} (kN. m/m)		Combinaisons			
		SLS_k−ENV	SLS_f−ENV	SLSqp−ENV	ULS−ENV
M_{xx}	Midspan	152.89	50.21	5.26	206.40
	Supports	76.01	26.03	1.05	102.61
M_{yy}	Midspan	208.15	119.80	68.33	280.10
	Supports	72.35	26.63	20.15	97.68

Table 13 ULS and SLS Actions in the Deck Slab.

Bending moments M_{Ed} (kN. m/m)			Combinaisons		
		SLS_k−ENV	SLS_f−ENV	SLSqp−ENV	ULS−ENV
M_{xx}	Midspan	152.89	50.21	5.26	206.40
	Supports	76.01	26.03	1.05	102.61
M_{yy}	Midspan	208.15	119.80	68.33	280.10
	Supports	72.35	26.63	20.15	97.68

At the ULS, the maximum midspan bending moments reach 206.40 kN·m/m in the (x-x) direction and 280.10 kN·m/m in the (y-y) direction. At the supports, the corresponding values are 102.61 kN·m/m and 97.68 kN·m/m, respectively. The (y-y) direction therefore governs the positive midspan bending moment, with a higher level of structural demand than that obtained in the (x-x) direction. This difference reflects the bidirectional distribution of loads within the deck slab and the contribution of the main girders to the transfer of vertical actions.

➢ *Deck Slab Reinforcement*

The calculated and adopted reinforcement areas are presented in Table 14.

For the bottom reinforcement layer, the calculated areas are 2851.19 mm²/m in the (x-x) direction and 3869.27 mm²/m in the (y-y) direction. A uniform adopted reinforcement area of 4021.25 mm²/m, corresponding to 5HA32, is provided in both directions.

For the top reinforcement layer, the calculated areas are 1417.44 mm²/m in the (x-x) direction and 1349.34 mm²/m in the (y-y) direction. An adopted reinforcement area of 1570.8 mm²/m, corresponding to 5HA20, is provided in both directions.

The use of identical reinforcement in both directions simplifies the detailing arrangement while maintaining a steel cross-sectional area greater than the calculated requirements.

Table 14 Deck Slab Reinforcement in the (x-x) and (y-y) Directions.

Reinforcement layer	Direction	Calculated area (mm²/m)	Adopted area (mm²/m)	Bars/m
Bottom layer	(x-x)	2851.19	4021.25	5HA32
	(y-y)	3869.27	4021.25	5HA32
Top layer	(x-x)	1417.44	1570.8	5HA20
	(y-y)	1349.34	1570.8	5HA20

➢ *Stress Verification in the Deck Slab*

The stress verification results are presented in Table 15. In the concrete, the maximum stresses are 16.22 MPa in the (x-x) direction and 15.16 MPa in the (y-y) direction, compared with an allowable limit of 21 MPa. The stresses in the reinforcement are 291.36 MPa and 277.96 MPa,

ISSN No:-2456-2165 https://doi.org/10.38124/ijisrt/26aug585

respectively, compared with an allowable limit of 400 MPa. All verification criteria are satisfied.

The concrete stress levels correspond to approximately 77% and 72% of the allowable limit in the two directions, respectively. For the reinforcement, the corresponding utilization levels are approximately 73% and 69%.

Table 15 Stress Verification in the Deck Slab in the (x-x) and (y-y) Directions.

Material	Direction	Stress, σ (MPa)	Allowable stress, σ_{adm} (MPa)	Condition $\sigma \leq \sigma adm$
Concrete	(x-x)	16.22	21	Verified
	(y-y)	15.16	21	Verified
Steel reinforcement	(x-x)	291.36	400	Verified
	(y-y)	277.96	400	Verified

➢ *Final Reinforcement Layout of the Bridge Deck*

Figure 7 presents the final reinforcement layout of the bridge deck resulting from the design of the main girders and the deck slab.

The graphical representation is consistent with the reinforcement areas adopted in Tables 9 and 14 and provides a visual representation of the distribution of longitudinal and transverse reinforcement within the different structural components of the deck.

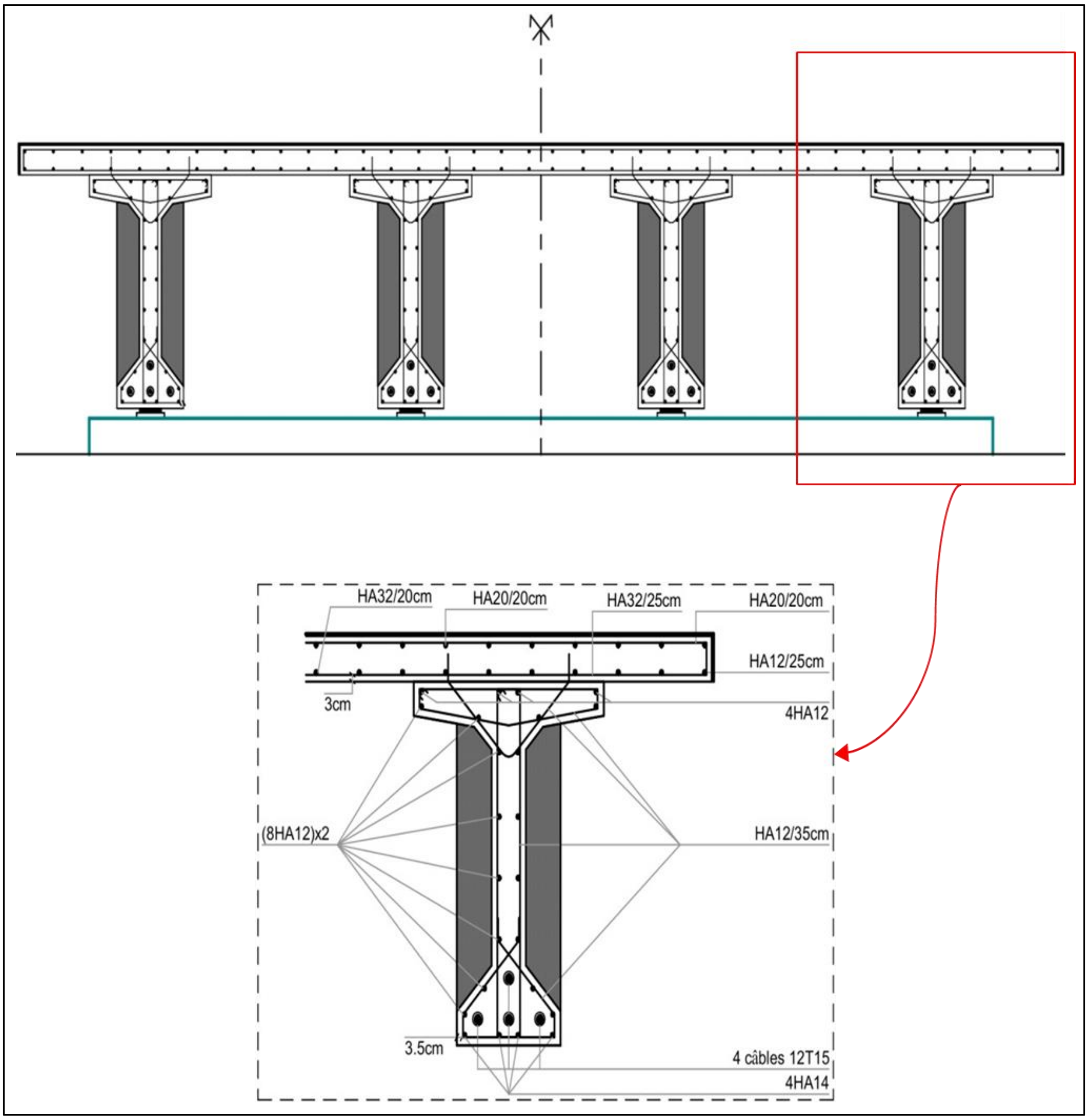

Fig 7 Final Reinforcement Layout of the Bridge Deck.

ISSN No:-2456-2165 https://doi.org/10.38124/ijisrt/26aug585

- *Discussion*

The results obtained show that the investigated bridge deck satisfies the strength and serviceability criteria considered in the analysis. The observed behavior is consistent with the role of prestressing in medium-span girder bridges, where the initial compressive stress introduced into the concrete helps limit tensile stresses and service-level deformations.

The maximum bending moment of 8.9423 MN·m and shear force of 1.3176 MN represent the governing design actions in the main girders. The obtained response justifies the use of a prestressed solution and leads to the adoption of four 12T15 tendons. This observation is consistent with the findings reported by Cheng (2013), Nguyen et al. (2022), and Williams et al. (2024), who highlighted the importance of prestressing in controlling the service behavior of prestressed concrete bridges.

The stress verification nevertheless shows that the available safety margin is not identical for all materials. Concrete exhibits the highest stress utilization, with 17.91 MPa compared with an allowable limit of 21 MPa. The prestressing steel reaches 1151 MPa compared with an allowable limit of 1422.9 MPa, whereas the passive reinforcement is mobilized to only approximately 23% of its allowable limit. This hierarchy is mechanically consistent with the respective roles of the different materials in a prestressed girder: the prestressing tendons provide a major contribution to flexural resistance, whereas passive reinforcement contributes particularly to local behavior, minimum reinforcement requirements, and structural robustness.

Time-dependent effects constitute a second important finding. The long-term creep coefficient of 1.8549 and the final shrinkage strain of -2.7539×10^{-4} demonstrate that concrete continues to evolve after its initial loading. This observation is consistent with the findings of Li et al. (2019), Nguyen et al. (2022), Williams et al. (2024), and Birhane et al. (2020), which highlight the influence of creep and shrinkage models on the prediction of long-term deformations in prestressed concrete structures.

This issue is particularly relevant to multi-span bridges. Nguyen et al. (2022) showed that the choice of creep and shrinkage model can lead to significant differences in the prediction of long-term deflection in prestressed concrete bridges. Similarly, Li et al. (2019) demonstrated that time-dependent behavior can simultaneously affect stresses and the global response of prestressed girders. These findings reinforce the relevance of explicitly considering time-dependent effects in the analysis of the investigated bridge.

For the deck slab, the difference between the bending moments obtained in the (x-x) and (y-y) directions, particularly at midspan, confirms the need for two-way reinforcement design. The adopted reinforcement area of 4021.25 mm²/m in the bottom layer provides sufficient coverage of the calculated requirements in both directions. The stress verification further confirms that the adopted reinforcement arrangement maintains the stress levels below the allowable limits.

The results are also consistent with studies addressing the reliability and long-term behavior of prestressed concrete bridges (Cheng, 2013; Teng et al., 2016; Zhou et al., 2023). These studies demonstrate that structural performance depends not only on initial strength but also on material evolution, prestress losses, and repeated actions throughout the service life.

The main contribution of the present study lies in the application of this approach to a real road bridge within the Cameroonian road network. The Bantoum Bridge therefore provides a case study linking regulatory requirements, numerical modeling, and the actual characteristics of a multi-span prestressed concrete bridge deck.

Nevertheless, the results should be interpreted within the scope of the study. The present analysis focuses primarily on the bridge deck. Therefore, it does not, by itself, allow conclusions to be drawn regarding the global safety of the entire structure, since the piers, bearings, and foundations were not subjected to detailed design verification.

A comprehensive assessment should also consider fatigue effects, repeated moving loads, progressive material deterioration, and the evolution of prestress losses throughout the service life. These aspects constitute natural extensions of the present study.

V. CONCLUSION

This study evaluated the structural behavior of the multi-span prestressed concrete deck of the Bantoum Bridge using numerical modeling in MIDAS Civil, considering permanent actions, road traffic loads, wind action, and time-dependent effects of concrete.

The results show that the maximum demands in the main girders remain compatible with the adopted prestressing system. The design leads to the adoption of four 12T15 tendons together with complementary passive reinforcement in the girders and deck slab. The ultimate and serviceability limit state verifications show that the stresses in concrete and reinforcement, as well as the deck deflection, remain below the considered design limits.

The analysis of time-dependent effects also highlights the influence of concrete creep and shrinkage on the long-term behavior of the deck. Their consideration is therefore an essential component of a realistic assessment of prestressed concrete structures.

Within the limitations of the adopted assumptions and the scope of the study, the results indicate that the investigated deck satisfies the considered strength and serviceability criteria. The study therefore provides a consistent numerical basis for the structural assessment of the deck of the Bantoum Bridge.

Future research should address the global assessment of the structure by incorporating the piers, bearings, and foundations; detailed analysis of prestress losses and long-term time-dependent effects; fatigue assessment under repeated traffic loading; comparison of numerical predictions with in-situ experimental measurements; and development of a structural health monitoring approach capable of anticipating changes in bridge performance and durability. These extensions would enable the transition from a numerical verification of the bridge deck toward a comprehensive and predictive assessment of the bridge performance throughout its service life.

REFERENCES

[1]. AFNOR. (2007). *Eurocodes – Bases de calcul des structures – Annexe nationale à la NF EN 1990/A1:2006 (NF EN 1990/A1/AN).* Association française de normalisation.

[2]. AFNOR. (2011). *Eurocodes – Bases de calcul des structures – Annexe nationale à la NF EN 1990:2003 (NF EN 1990/AN).* Association française de normalisation.

[3]. AFNOR. (2011). *Aciers de précontrainte – Partie 1: Prescriptions générales (XP A35-045-1).* Association française de normalisation.

[4]. AFNOR. (2011). *Aciers de précontrainte – Partie 2: Fils (XP A35-045-2).* Association française de normalisation.

[5]. AFNOR. (2011). *Aciers de précontrainte – Partie 3: Torons (XP A35-045-3).* Association française de normalisation.

[6]. AFNOR. (2011). *Aciers de précontrainte – Partie 4: Barres (XP A35-045-4).* Association française de normalisation.

[7]. AFNOR. (2014). *Béton – Spécification, performances, production et conformité (NF EN 206/CN).* Association française de normalisation.

[8]. Birhane, F. N., Kim, S.-I., & Jang, S. Y. (2020). Long-term deflection of prestressed concrete bridge considering nonuniform shrinkage and crack propagation by equivalent load approach. *Journal of Bridge Engineering*. https://doi.org/10.1061/(ASCE)BE.1943-5592.0001370

[9]. Cheng, J. (2013). Serviceability reliability analysis of prestressed concrete bridges. *KSCE Journal of Civil Engineering, 17*(2), 415–425. https://doi.org/10.1007/s12205-013-1374-x

[10]. CEN. (2003). *EN 1990: Eurocode – Basis of structural design.* European Committee for Standardization.

[11]. CEN. (2005). *EN 1992-1-1: Eurocode 2 – Design of concrete structures – Part 1-1: General rules and rules for buildings.* European Committee for Standardization.

[12]. CEN. (2006). *EN 1992-2: Eurocode 2 – Design of concrete structures – Concrete bridges – Design and detailing rules.* European Committee for Standardization.

[13]. CEN. (2007). *Designers' Guide to EN 1992-2: Eurocode 2 – Design of concrete structures – Part 2: Concrete bridges.* Thomas Telford.

[14]. Freyssinet, E. (1950). Prestressed concrete: Principles and applications. *Journal of the Institution of Civil Engineers, 33*(4), 551–580.

[15]. Freyssinet, E. (1966). *Exposé d'ensemble de l'idée de précontrainte.* Travaux, 375, 327–?.

[16]. Ghali, A., & Elbadry, M. M. (1989). Serviceability design of continuous prestressed concrete structures. *PCI Journal.*

[17]. Gilbert, R. I., Mickleborough, N. C., & Ranzi, G. (2017). *Design of Prestressed Concrete to Eurocode 2* (2nd ed.). CRC Press. https://doi.org/10.1201/9781315389516

[18]. Hewson, N. R. (2011). *Prestressed Concrete Bridges: Design and Construction* (2nd ed.). ICE Publishing. https://doi.org/10.1680/pcb.41134

[19]. Li, S., Yang, Y., Pu, Q., Yang, D., Sun, B., & Li, X. (2019). Three-dimensional nonlinear creep and shrinkage effects of a long-span prestressed concrete box girder bridge. *Structural Concrete, 20*(2), 638–649. https://doi.org/10.1002/suco.201800148

[20]. Luo, H., Xu, C., Gan, X., Liu, M., Guo, X., & Guo, H. (2022). The train-bridge coupled vibration analysis of a long-span prestressed concrete continuous beam bridge under creep deformation effect. *Applied Sciences, 12*(22), 11838. https://doi.org/10.3390/app122211838

[21]. Nguyen, X. T., Ngo, V. M., Nguyen, N. L., & Pham, T. D. (2022). Effect of creep and shrinkage model in calculation of long-term deflection of three-span solid slab continuous prestressed concrete bridge. *Journal of Materials and Engineering Structures, 9*, 427–434.

[22]. Teng, Tong., Zhao, L., Zhang, J., & Yu, Q. (2016). Long-term performance of prestressed concrete bridges under the intertwined effects of concrete damage, static creep and traffic-induced cyclic creep. *Engineering Structures, 127*, 510–524. https://doi.org/10.1016/j.engstruct.2016.09.004

[23]. Williams, M., Menon, D., & Prasad, A. M. (2024). Creep and shrinkage in prestressed concrete beams: An experimental study. *Structural Concrete*. https://doi.org/10.1002/suco.202300625

[24]. Zhou, H., Fan, X., Liu, Y., & Lu, D. (2023). Time-variant reliability analysis of simply supported PC girder bridges considering shrinkage, creep, resistance degradation and vehicle load flows. *Engineering Structures.*